

Improving the Efficiency of Self-Supervised Adversarial Training through Latent Clustering-Based Selection

Somrita Ghosh
CISPA Helmholtz Center for
Information Security
somrita.ghosh@cispa.de

Yuelin Xu
CISPA Helmholtz Center for
Information Security
yuelin.xu@cispa.de

Xiao Zhang
CISPA Helmholtz Center for
Information Security
xiao.zhang@cispa.de

Abstract

Compared with standard learning, adversarially robust learning is widely recognized to demand significantly more training examples. Recent works propose the use of self-supervised adversarial training (SSAT) with external or synthetically generated unlabeled data to enhance model robustness. However, SSAT requires a substantial amount of extra unlabeled data, significantly increasing memory usage and model training times. To address these challenges, we propose novel methods to strategically select a small subset of unlabeled data essential for SSAT and robustness improvement. Our selection prioritizes data points near the model’s decision boundary based on latent clustering-based techniques, efficiently identifying a critical subset of unlabeled data with a higher concentration of boundary-adjacent points. While focusing on near-boundary data, our methods are designed to maintain a balanced ratio between boundary and non-boundary data points to avoid overfitting. Our experiments on image benchmarks show that integrating our selection strategies into self-supervised adversarial training can largely reduce memory and computational requirements while achieving high model robustness. In particular, our latent clustering-based selection method with k-means is the most effective, achieving nearly identical test-time robust accuracies with 5 to 10 times less external or generated unlabeled data when applied to image benchmarks. Additionally, we validate the generalizability of our approach across various application scenarios, including a real-world medical dataset for COVID-19 chest X-ray classification. Our Implementations are available as open-source code at [this url](#).

1 Introduction

Over the past decade, it has been repeatedly confirmed that deep neural networks (DNNs) are highly vulnerable to adversarial perturbations [35]. This phenomenon has raised serious concerns about the reliability of DNNs in safety-critical applications and has driven numerous research into designing methods to enhance model robustness [3, 4, 13, 26]. Among them, adversarial training is regarded as one of the most effective methods [22, 38, 45]. However, as stated by Schmidt et al. [29], learning a model that is resilient to adversarial perturbations requires a significantly larger dataset than standard learning. Recent studies have explored self-supervised techniques to expand the training set size of adversarial training algorithms by leveraging unlabeled external [6] or generated data [15, 30, 39]. Despite alleviating the sample complexity barrier and producing models with improved robust accuracies, these methods typically utilize vast amounts of additional data, suggesting the requirement of much larger hardware to store those data and a much longer training time for algorithms like adversarial training to converge.

Witnessing the challenges of additional memory and computational requirements, we investigate *whether the significantly large amount of utilized additional data is inevitable for achieving state-of-the-art adversarial robustness*. The ultimate goal of our work is to maximize the model robustness achieved by SSAT algorithms by using as few additional unlabeled data points as possible. Inspired by Zhang et al. [46], which highlights the unequal importance of training examples, we argue that with limited model capacity, self-supervised adversarial learning should also focus on optimizing critical data samples near the model’s decision boundary. Consequently, we propose multiple data selection strategies, including a simple *prediction confidence-based selection* (PCS) scheme that prioritizes unlabeled data points in which the model’s prediction is most uncertain and more advanced *latent clustering-based selection* (LCS) schemes. Specifically, we propose two LCS approaches depending on the corresponding clustering technique it builds on: *latent clustering-based selection with Gaussian mixture models* (LCS-GMM) and *latent clustering-based selection with k-means* (LCS-KM). For each unlabeled data point, we compute the difference between the highest and second-highest posterior probabilities in the latent feature space for LCS-GMM, while we select vulnerable points by calculating the distance difference between the two nearest cluster centroids for LCS-KM. The set of unlabeled data with the smallest probability or distance difference is considered more critical and further incorporated into self-supervised adversarial training. Moreover, our selection strategies balance the ratio of boundary critical points and the remaining non-boundary points to avoid undesirable overfitting to the boundary data distribution.

By applying these targeted data reduction approaches, we streamline the self-supervised adversarial training process, significantly reducing the required additional unlabeled data while maintaining comparable model robustness against adversarial perturbations. Our work offers valuable insights into how to acquire additional data and employ SSAT in resource-constrained application domains. Below, we further summarize the main contributions of our work.

Contributions. We motivate and formalize the problem task of reducing the volume of unlabeled data while maintaining model robustness for SSAT (Section 3). To realize such a goal, we propose various data selection schemes to identify the most critical unlabeled data points, including a straightforward approach based on prediction confidence and two advanced methods based on clustering techniques of unlabeled data in the latent embedding space (Section 4). The proposed methods optimize the performance of SSAT by refining the model’s decision boundary in the input regions of high uncertainty by strategically prioritizing boundary-adjacent unlabeled data points. By focusing on critical unlabeled data points, our methods largely reduce the memory consumption and time

complexities of self-supervised adversarial training algorithms. We conduct comprehensive experiments on two image benchmarks and a real-world medical dataset, demonstrating that our data selection schemes significantly reduce the memory consumption and the total running time of self-supervised adversarial training algorithms under various experimental settings (Section 5). Additionally, we explain the insights of the potential reasoning behind the superior efficacy of our LCS-KM method to other data selection schemes (Section 6.1) and provide general guidelines on how to employ our LCS methods for maximized robustness performance (Section 6.2). Finally, we examine the robustness of our methods by varying the adversarial training algorithms, perturbation size and metric (Section 6.3), as well as studying the role of the intermediate model under the regime with insufficient labeled data (Section 6.4), all confirming the usefulness and generalizability of the proposed data selection schemes for improving the efficiency of SSAT algorithms. We believe our work can help promote the development of more scalable, robust learning algorithms, which would be particularly beneficial for resource-constrained environments.

2 Related Work

In this section, we review the most relevant literature on adversarial examples, (self-supervised) adversarial training, and its variants. We also discuss the most representative techniques for improving the efficiency of standard deep learning, including dataset distillation and coreset selection.

2.1 Adversarially Robust Learning

Adversarial Examples. Adversarial examples are inputs crafted with small perturbations that are designed to mislead model predictions [35]. The prevalence of adversarial examples with deep neural networks poses a critical challenge in modern machine learning, especially for security-critical or safety-critical applications. Earlier-proposed attacks like fast gradient sign method (FGSM) [13] and projected gradient descent (PGD) [22] introduced gradient-based techniques to find adversarial examples using constrained optimization, while Carlini and Wagner proposed unconstrained CW attacks [5], which search for the minimal perturbation that causes misclassification. Recent attacks like Auto-PGD [9] automate gradient steps for higher efficiency in finding worst-case perturbations, while AutoAttack [8] is an ensemble of diverse parameter-free attacks, making them more effective in evaluating model robustness.

Adversarial Training. On the defense side, adversarial training and its variants are the most popular learning methods for adversarial robustness. For instance, Madry et al. proposed to train DNNs on adversarially perturbed inputs using PGD attacks [22], while Zhang et al. introduced TRADES [45], which balances the trade-off between adversarial robustness and standard accuracy. Nevertheless, adversarial training algorithms are often criticized for overfitting adversarially perturbed samples produced during training time and for their high computation costs, which hinder their deployment in real-world applications. In particular, Rice et al. illustrated through comprehensive experiments that the robust overfitting phenomenon is prevalent in adversarial training [28], where early stopping is shown to be effective in alleviating such an issue. Techniques,

such as Free AT [32] and Fast AT [40], offer promising solutions to reduce the computation for adversarial training. Nevertheless, they suffer from decreased robustness performance.

Moreover, a line of research pointed out that treating all the data points equally in adversarial training is not optimal for robust learning since different examples can impact model robustness differently. For example, Zhang et al. argued that data points far from decision boundaries are inherently more secure and less likely to be influential in robust learning against adversarial perturbations [46]. As a result, these points should be given less weight during training to prevent the model from overfitting them, which could negatively affect its generalization on more vulnerable or unseen data. In a similar vein, Hua et al. advocated for a more targeted approach [18], recommending that PGD training be applied primarily to examples situated near the decision boundaries. This strategy focuses the model’s attention on the points that are most likely to enhance its robustness, as adversarial perturbations on boundary-adjacent data are more likely to result in meaningful improvements to the model’s resistance to attacks. Our work builds on these ideas by strategically identifying and prioritizing boundary-adjacent points from the unlabeled dataset to address the unique challenges associated with self-supervised adversarial training methods.

Self-Supervised Adversarial Training. Utilizing unlabeled data to improve model performance has become an active and rapidly advancing field of research [7]. In the adversarial context, Schmidt et al. [29] highlighted a key observation: the sample complexity required for robust learning far exceeds that of standard learning. They showed that achieving adversarially robust generalization often necessitates a much larger dataset than traditional learning approaches, posing a challenge when labeled data is scarce or costly. Subsequently, a line of works proposed to boost model robustness by involving additional unlabeled data, often acquired from a similar but slightly different distribution, using self-supervised methods in adversarial training [1, 6, 24, 44]. In particular, Carmon et al. proposed robust self-training methods to address the sample complexity issue [6], which first trains an intermediate model using available labeled data and then leverages the model to generate pseudo-labels for unlabeled data. The pseudo-labeled samples, combined with the original labeled data, are subsequently used to train a final robust model. Concurrently, Najafi et al. proposed an optimization framework incorporating labeled and unlabeled data [24], while providing formal guarantees on adversarial robustness.

In addition, leveraging synthetic data produced by state-of-the-art generative models to build robust models has also been explored extensively in recent literature [15, 30, 39]. For instance, Goyal et al. employed various unconditional generative models [15], including variational autoencoders (VAEs), generative adversarial networks (GANs), and the more advanced denoising diffusion probabilistic models (DDPMs), to produce a large synthetic dataset to be incorporated in adversarial training, which improves robustness further. While all the aforementioned SSAT methods enrich the training dataset, they require considerable additional unlabeled data to ensure effective robustness enhancement. In this work, we explore data selection schemes to reduce the amount of unlabeled or generated data that are both efficient and effective for self-supervised adversarial training to achieve good robustness performance.

2.2 Data-Efficient Deep Learning

Within the broader literature of data-efficient deep learning, various techniques have been proposed to reduce the amount of training data while retaining critical information. Two prominent approaches are dataset distillation and coreset selection.

Dataset Distillation. Dataset distillation compresses large datasets into compact, synthetic datasets by matching gradients or optimizing specific loss functions, allowing models to achieve comparable performance with significantly fewer data points. For instance, Wang et al. proposed a foundational approach to dataset distillation [37], proposing methods to condense large datasets into smaller, synthetic subsets while preserving model performance. Later, Zhao et al. introduced the concept of gradient matching [47], where distilled data points are optimized to match the gradients of the original dataset. This technique largely improves the distillation performance, enabling models to learn more effectively from reduced data. Additionally, Sucholutsky and Schonlau proposed soft-label dataset distillation, which uses probabilistic labels for distilled data [34], facilitating the training of complex models with minimal data while maintaining strong performance. Despite its success in standard deep learning, dataset distillation is often impractical for robust learning due to its high computational demands. Moreover, it assumes that all the examples in the entire dataset are equally important for distillation, ignoring the fact that different data points may have varying influences on model performance.

Coreset Selection. On the other hand, coreset selection [20, 31] aims to identify a small, representative data subset that retains the model performance when trained on this reduced dataset. These approaches often rely on diversity-based metrics or optimization techniques to ensure that the selected subset preserves sufficient information for effective learning. For example, Kaushal et al. utilized diverse models to select training data subsets to reduce labeling efforts [19], while Xia et al. introduced the concept of “moderate coreset” [42], focusing on data points with scores near the median to construct subsets that generalize well across different scenarios based on score distributions. Similarly, Mirzasoleiman et al. proposed selecting a weighted subset of training data that approximates the full gradient by maximizing a submodular function [23].

In the adversarial context, Dolatabadi et al. proposed adversarial coreset selection [11], offering a task-specific solution to enhance the computational efficiency of adversarial training. In particular, the method constructs a compact data subset by minimizing the gradient approximation error. The constructed subset is then utilized for adversarial training, with selection taking place at regular intervals. While effective in reducing computational overhead for vanilla adversarial training, the growing reliance on large volumes of generated or external data—such as in self-supervised adversarial training—introduces new challenges. These approaches often expand the dataset size to improve robust accuracy, eventually increasing the total training time. In such settings, repeatedly selecting data during training may become computationally infeasible. In summary, our work complements the above-mentioned methods for efficient deep learning, focusing on developing more data selection schemes without compromising robustness or scalability, particularly for SSAT when large-scale unlabeled data are involved.

3 Improving Data Efficiency for SSAT

In this section, we first introduce the necessary notations and definitions for readers to understand self-supervised adversarial training (Section 3.1) and then motivate and formulate the problem task of enhancing the data efficiency of SSAT algorithms (Section 3.3).

3.1 Preliminaries on SSAT

We work with self-supervised adversarial training algorithms, initially introduced to the field by Carmon et al. [6]. Let $\mathcal{X} \subseteq \mathbb{R}^n$ be a n -dimensional input space, \mathcal{Y} be the output space of class labels, and D_l be the underlying labeled distribution supported on $\mathcal{X} \times \mathcal{Y}$ that we aim to learn an adversarially robust classifier. Let \mathcal{S}_l be the training set with examples i.i.d. drawn from D_l and \mathcal{S}_u be a set of inputs sampled from some unlabeled distribution D_u supported on \mathcal{X} . In the adversarial machine learning literature, D_u is typically considered to be similar but not identical to the marginal input distribution of D_l , and $|\mathcal{S}_u|$ is set to be much larger than $|\mathcal{S}_l|$, since unlabeled data are easier to acquire than well-annotated labeled data. Throughout the paper, we use $|\cdot|$ to denote the cardinality of the corresponding set. For instance, when \mathcal{S}_l corresponds to the 50K labeled CIFAR-10 training images, Carmon et al. [6] selected 500K “most CIFAR-10-like but non-identical” images from the whole 80M Tiny ImageNet data as the unlabeled dataset \mathcal{S}_u to be used by SSAT.

To be more specific, SSAT first standardly trains an intermediate model $f_{\hat{\theta}}$ on \mathcal{S}_l , known as the *pseudo labeling function*, and then assigns pseudo-labels to each unlabeled data point $\mathbf{x} \in \mathcal{S}_u$. More rigorously, the intermediate model’s weight parameters $\hat{\theta}$ are learned by minimizing the following objective function:

$$\hat{\theta} = \operatorname{argmin}_{\theta} \frac{1}{|\mathcal{S}_l|} \sum_{(\mathbf{x}, y) \in \mathcal{S}_l} \mathcal{L}(\theta, \mathbf{x}, y), \quad (1)$$

where $\mathcal{L}(\cdot)$ denotes the standard loss, such as cross-entropy, that measures the discrepancy between model prediction and the class label. Finally, SSAT trains a model, denoted as $\text{SSAT}(\mathcal{S}_l, \mathcal{S}_u, \gamma)$, on both labeled dataset \mathcal{S}_l and unlabeled dataset \mathcal{S}_u but paired with pseudo labels by minimizing the following adversarial loss:

$$\min_{\theta} \frac{1}{|\mathcal{S}_l|} \sum_{(\mathbf{x}, y) \in \mathcal{S}_l} \mathcal{L}_{\text{adv}}(\theta, \mathbf{x}, y) + \frac{1}{\gamma |\mathcal{S}_u|} \sum_{\mathbf{x} \in \mathcal{S}_u} \mathcal{L}_{\text{adv}}(\theta, \mathbf{x}, f_{\hat{\theta}}(\mathbf{x})), \quad (2)$$

where $\gamma \geq 0$ controls the contributions between labeled and unlabeled data. In prior literature [15], a typical approach is to construct each training batch with varying ratios of labeled and unlabeled data (corresponding to different values of α) but fix the total batch size to optimize for the best SSAT performance. For simplicity, we term γ as the per-batch ratio hyperparameter in this paper. When $\frac{1}{\gamma}$ is set as 0, Equation 2 reduces to the training objective of vanilla adversarial training (AT) [22]. In Equation 2, $\mathcal{L}_{\text{adv}}(\cdot)$ stands for the adversarial loss function: for any $(\mathbf{x}, y) \in \mathcal{S}_l$ and $\epsilon > 0$,

$$\mathcal{L}_{\text{adv}}(\theta, \mathbf{x}, y) = \max_{\delta \in \mathcal{B}_{\epsilon}(\mathbf{0})} \mathcal{L}(\theta, \mathbf{x} + \delta, y), \quad (3)$$

where $\mathcal{B}_{\epsilon}(\mathbf{0})$ denotes the ball centered at $\mathbf{0}$ with radius ϵ measured in some distance metric, such as ℓ_p -norm. Aligned with prior literature on adversarial training [22], we adopt multi-step PGD to obtain an approximated solution to the inner maximization problem specified by Equation 3 during self-supervised adversarial training.

3.2 Limitations of Existing SSAT Methods

Although SSAT methods alleviate the sample complexity barriers of adversarially robust learning [29] and can produce models with higher robust accuracies, they require a substantial amount of extra unlabeled data \mathcal{S}_u to ensure effective robustness enhancement. This trend is clearly documented in the leaderboard of RobustBench [8]. For example, state-of-the-art SSAT methods [6, 15, 39] either select 500K external Tiny Imagenet data samples or generate millions of synthetic CIFAR-10-like images, both significantly larger than the original 50K CIFAR-10 training examples. For example, the method proposed by Gowal et al. [15] achieves around 65% robust accuracy on CIFAR-10 using a WideResNet-70-16 model architecture against ℓ_∞ perturbations with $\epsilon = 8/255$, increasing the robustness performance of vanilla adversarial training [22] by a large margin, but relies on an extra unlabeled set of 100M DDPM-generated data. The huge unlabeled dataset required for SSAT significantly increases memory consumption for holding the whole training dataset, which we argue is inefficient and likely to be prohibited for resource-constrained application scenarios. These observations motivate us to explore whether such a considerable amount of unlabeled data can be reduced while preserving the high model robustness attained by SSAT algorithms.

Moreover, we note that SSAT requires a much longer convergence time to obtain the best-performing model, usually 2 to 4 times the number of training epochs compared with vanilla AT (see Figure 1 for supporting evidence). Intuitively, extracting useful and robust features through adversarial training from such a large and potentially diverse dataset is more difficult. As we will illustrate in our experiments, the slower convergence can be attributed to the additional large unlabeled datasets (with pseudo labels) that often exhibit higher variance than the original labeled data samples. Once we reduce the size of the unlabeled data involved with specifically designed techniques, faster convergence is expected for SSAT. Since vanilla adversarial training has already been criticized in prior literature [32, 40] for its high computational costs for running multi-step PGD to solve the inner maximization problem in Equation 3, state-of-the-art SSAT algorithms incur even higher computational costs (see Table 1 for runtime comparisons), due to the slower convergence rate and larger model architecture they typically adopt. Therefore, it is essential to design efficient SSAT methods, especially for resource-constrained applications, that can better utilize the large amount of extra unlabeled data.

3.3 Problem Formulation

Witnessing the data and computational inefficiency of SSAT methods, we propose to study whether the large set size of unlabeled data is inevitable for training models with good robustness performance. Inspired by the idea of coreset selection for efficient deep learning [19, 23, 42], we propose to strategically search for a small but essential set of unlabeled data $\mathcal{A}_u \subseteq \mathcal{S}_u$ such that self-supervised adversarial training based on \mathcal{S}_l and the selected subset \mathcal{A}_u can produce models with comparable robustness to those obtained using full unlabeled dataset \mathcal{S}_u . More formally, we aim to solve the following constrained optimization problem:

$$\max_{\mathcal{A}_u \subseteq \mathcal{S}_u} \text{AdvRob}_\epsilon(\text{SSAT}(\mathcal{S}_l, \mathcal{A}_u, \gamma)), \text{ s.t. } |\mathcal{A}_u| \leq \alpha |\mathcal{S}_u|, \quad (4)$$

where $\text{SSAT}(\mathcal{S}_l, \mathcal{A}_u, \gamma)$ stands for the model learned by SSAT with \mathcal{S}_l and \mathcal{A}_u based on Equation 2, and $\alpha \in (0, 1)$ is a predefined ratio capturing the data constraint. $\text{AdvRob}_\epsilon(\theta)$ denotes the robustness of the model with parameters θ against ϵ perturbations:

$$\text{AdvRob}_\epsilon(\theta) = 1 - \mathbb{E}_{(\mathbf{x}, y) \sim D_l} \left[\max_{\delta \in \mathcal{B}_\epsilon(\mathbf{0})} \mathcal{L}_{0/1}(\theta, \mathbf{x} + \delta, y) \right] \quad (5)$$

where $\mathcal{L}_{0/1}$ denotes the 0-1 loss function. Due to the combinatorial nature and the high computation costs of AT algorithms, it is computationally hard to enumerate all the feasible subsets \mathcal{A}_u to solve the proposed optimization problem exactly. As we will illustrate in the following sections, we design different data selection schemes with respect to the extra unlabeled dataset for SSAT that are effective in approximately solving the optimization problem in Equation 4 while only incurring negligible computational overhead.

4 Proposed Data Selection Schemes

So far, we have introduced the problem task of reducing the unlabeled dataset size to improve the efficiency of SSAT algorithms while maintaining the robustness enhancement and illustrated its importance. Motivated by the significant role of boundary-adjacent data points in optimizing model performance (Section 4.1), in this section, we design three efficient data selection schemes to address the optimization problem in Equation 4 (Sections 4.2 and 4.3).

4.1 Prioritize Boundary Unlabeled Data

Achieving high model robustness with restricted data resources remains a challenging task in machine learning. It involves striking a balance among data significance, optimizing the use of labeled and unlabeled data, and tackling constraints imposed by model capacity. Inspired by the prior literature [18, 46] that emphasizes the imbalanced data importance for vanilla adversarial training (see Section 2.1 for detailed discussions of these works), we hypothesize that not all unlabeled data contribute equally to the robustness enhancement for SSAT. In particular, we propose identifying a small set of *vulnerable yet valuable* unlabeled data points in \mathcal{S}_u , which are close to the model’s decision boundary. Consequently, such boundary-adjacent data points are highly susceptible to label changes under small input perturbations and are inherently difficult for the model to classify. Thus, improving their classification can yield more robustness enhancement to adversarial inputs. We expect the decision boundary of the intermediate model $f_{\hat{\theta}}$ to act as an effective proxy for locating difficult-to-classify data points. Since the intermediate model is usually trained with strong standard accuracy, it is expected to preserve class semantics and provide a solid foundation for identifying these critical points. SSAT algorithms can then leverage this information to ensure these boundary-adjacent points are correctly classified, even under adversarial conditions. By focusing more on these critical boundary points with respect to the intermediate model, the final model can be trained more efficiently using SSAT algorithms while upholding robust accuracies (see Figure 7 in Appendix A for an illustration of the overall training pipeline).

While a straightforward extension of existing approaches is to select unlabeled data based on how much their predictions change under perturbations found by PGD attacks, this method is computationally expensive, undermining the efficiency gains we seek.

Algorithm 1 Prediction Confidence-based Selection

-
- 1: **Input:** labeled dataset \mathcal{S}_l ; unlabeled dataset \mathcal{S}_u ; selection ratio α ; perturbation size ϵ ; boundary ratio β ; per-batch ratio γ
 - 2: $\hat{\theta} \leftarrow$ train a standard classification model on \mathcal{S}_l
 - 3: $\hat{y} \leftarrow$ predict pseudo label $f_{\hat{\theta}}(\mathbf{x})$ for $\mathbf{x} \in \mathcal{S}_u$
 - 4: Initialize \mathcal{A}_u as empty set
 - 5: $\text{Conf}(\mathbf{x}) \leftarrow$ get confidence of $f_{\hat{\theta}}(\mathbf{x})$ for $\mathbf{x} \in \mathcal{S}_u$
 - 6: Sort \mathcal{S}_u by ascending order of $\text{Conf}(\mathbf{x})$
 - 7: $\mathcal{A}_u \leftarrow$ add top $\beta \cdot \alpha |\mathcal{S}_u|$ points with lowest $\text{Conf}(\mathbf{x})$
 - 8: $\mathcal{A}_u \leftarrow$ add $(1 - \beta) \cdot \alpha |\mathcal{S}_u|$ points randomly from $\mathcal{S}_u \setminus \mathcal{A}_u$
 - 9: $\theta_{\text{final}} \leftarrow$ SSAT($\mathcal{S}_l, \mathcal{A}_u, \gamma$) based on Equation 2
 - 10: **Output:** selected subset \mathcal{A}_u , final model θ_{final}
-

Specifically, these methods entail iterative optimization processes to pinpoint boundary points, making them less efficient, especially for large-scale datasets. Additionally, while these methods provide valuable insights, their complexity often limits their interpretability. Therefore, we seek alternatives to effectively identify boundary data points without incurring high computational overhead.

4.2 Prediction Confidence-Based Selection

To identify the critical set of vulnerable data points near the model’s decision boundary while accounting for computational efficiency, scalability, and interpretability, we first propose a straightforward approach, termed as *Prediction Confidence-based Selection* (PCS), which utilizes the intermediate model $f_{\hat{\theta}}$ to compute a prediction confidence score for each unlabeled data point. The pseudocode for such a selection scheme is depicted in Algorithm 1. Initially, all the data points in \mathcal{S}_u are sorted by their prediction confidence $\text{Conf}(\cdot)$, with those exhibiting the lowest confidence scores being prioritized. The underlying assumption is that data points with low confidence scores are more likely to lie near the decision boundary, making them ideal candidates for our selection. Note that the parameter $\beta \in [0, 1]$ is introduced to balance the ratio between boundary and non-boundary points to avoid overfitting, which is used in all our proposed selection schemes. The reason for involving such a trade-off parameter will be further discussed in Section 6.2.

The biggest advantage of PCS is its high computational efficiency for ranking the unlabeled data using model confidence scores. Note that for self-supervised adversarial training, we usually have an order-wise larger collection of unlabeled data than the original labeled dataset. Thus, an efficient data selection scheme is desirable to avoid high computational overhead. Nevertheless, we discovered in our experiments that using prediction confidence may not capture the underlying structure of the data well, leading to decreased robustness enhancement when incorporated in SSAT. We hypothesize that PCS overlooks the geometric relationships and distributional properties, which are crucial for characterizing boundary-adjacent points, particularly for complex datasets. In addition, DNNs have been shown to be overconfident in their predictions [16], suggesting prediction confidence score might be an inherently biased indicator.

4.3 Latent Clustering-Based Selection

To overcome the above issues, we propose *latent clustering-based selection* (LCS) strategies, which identify data points near the model’s

Algorithm 2 Latent Clustering-based Selection

-
- 1: **Input:** labeled dataset \mathcal{S}_l ; unlabeled dataset \mathcal{S}_u ; selection ratio α ; cluster number k ; perturbation size ϵ ; boundary ratio β ; per-batch ratio γ
 - 2: $\hat{\theta} \leftarrow$ train a standard classification model on \mathcal{S}_l
 - 3: $\hat{y} \leftarrow$ predict pseudo label $f_{\hat{\theta}}(\mathbf{x})$ for $\mathbf{x} \in \mathcal{S}_u$
 - 4: Initialize \mathcal{A}_u as empty set
 - 5: $\mathbf{z} \leftarrow$ get latent embeddings $h_{\hat{\theta}}(\mathbf{x})$ for $\mathbf{x} \in \mathcal{D}_u$
 - 6: **if** using LCS-KM **then**
 - 7: $\{C_1, \dots, C_k\} \leftarrow$ k-means clustering on $\{\mathbf{z}\}_{\mathbf{x} \in \mathcal{S}_u}$
 - 8: $\Delta d \leftarrow$ compute $\Delta d = |d_1 - d_2|$ for $\mathbf{x} \in \mathcal{D}_u$, where d_1 and d_2 are Euclidean distances to the nearest two centroids
 - 9: $\mathcal{A}_u \leftarrow$ add top $\beta \cdot \alpha |\mathcal{S}_u|$ points with smallest Δd
 - 10: **else if** using LCS-GMM **then**
 - 11: Fit a GMM with k components to $\{\mathbf{z}\}_{\mathbf{x} \in \mathcal{S}_u}$
 - 12: Compute posterior probabilities $\mathbf{p}(\mathbf{z})$ for each \mathbf{z}
 - 13: $\Delta p \leftarrow$ compute $\Delta p = |p_1 - p_2|$ for each \mathbf{z} , where p_1 and p_2 are the top two highest probabilities
 - 14: $\mathcal{A}_u \leftarrow$ add top $\beta \cdot \alpha |\mathcal{S}_u|$ points with smallest Δp
 - 15: **end if**
 - 16: $\mathcal{A}_u \leftarrow$ add $(1 - \beta) \cdot \alpha |\mathcal{S}_u|$ points randomly from $\mathcal{S}_u \setminus \mathcal{A}_u$
 - 17: $\theta_{\text{final}} \leftarrow$ SSAT($\mathcal{S}_l, \mathcal{A}_u, \gamma$) based on Equation 2
 - 18: **Output:** selected dataset \mathcal{A}_u , final model θ_{final}
-

decision boundary in the latent space using different clustering techniques. Our approach begins by generating latent embeddings for all unlabeled data $\mathbf{z} = h_{\hat{\theta}}(\mathbf{x})$, where $h_{\hat{\theta}}$ denotes the mapping of the input layer to the penultimate layer with respect to the intermediate model $f_{\hat{\theta}}$. The penultimate layer captures more abstract, high-level features and better represents the underlying data structure, which helps identify points near decision boundaries. It avoids the biases of overconfident predictions from the final layer, offering more reliable clustering. Here, the goal is to identify boundary-adjacent data points inferred by examining distances to cluster centroids. Points equidistant from multiple centroids are expected to be closer to decision boundaries in the latent embedding space.

In particular, we explore two classical clustering techniques for their unique benefits in identifying boundary points in the LCS framework. Algorithm 2 presents the pseudocode of the two proposed LCS methods. In particular, *LCS with k-means* (LCS-KM) generates latent representations of unlabeled data and clusters them based on Euclidean distances to the centroids, prioritizing data points that are equidistant from multiple centroids to capture local geometric structures around decision boundaries effectively. On the other hand, *LCS with Gaussian mixture models* (LCS-GMM) fits the latent representations to Gaussian mixture models, using posterior probabilities across multiple fitted Gaussians to identify points that are likely near decision boundaries. Compared to PCS, both LCS-KM and LCS-GMM leverage latent space clustering to provide a more accurate characterization of boundary vulnerabilities.

LCS-KM. In this variant of LCS, we first generate latent embeddings $\{\mathbf{z} = h_{\hat{\theta}}(\mathbf{x}) : \mathbf{x} \in \mathcal{S}_u\}$, and then partition the N unlabeled data points into k clusters $\{C_1, C_2, \dots, C_k\}$ by minimizing the within-cluster sum of squares $\sum_{j=1}^k \sum_{\mathbf{z} \in C_j} \|\mathbf{z} - \boldsymbol{\mu}_j\|^2$, where $\boldsymbol{\mu}_j$ is the centroid of the j -th cluster. For each latent embedding \mathbf{z} , we compute the Euclidean distance to each cluster centroid $\|\mathbf{z} - \boldsymbol{\mu}_j\|$. Data

points are selected based on the minimal difference in distance between each latent embedding \mathbf{z} to the corresponding two closest cluster centroids $\Delta d = |d_1 - d_2|$, where d_1 and d_2 are the Euclidean distances to the closest and second closest centroids, respectively. The set of unlabeled inputs with the smallest Δd values are selected. Finally, the top $\alpha|\mathcal{S}_u|$ points from \mathcal{S}_u with the smallest Δd values form the reduced unlabeled dataset followed by the same balancing step using the ratio parameter β . As will be demonstrated in our experiments, prioritizing these strategically selected unlabeled data points during self-supervised adversarial training can achieve comparable robustness with much-improved efficiency.

LCS-GMM. In this variant of LCS, we again start by computing latent embeddings for unlabeled data $\{\mathbf{z} = h_{\hat{\theta}}(\mathbf{x}) : \mathbf{x} \in \mathcal{S}_u\}$. Instead of using k-means clustering, we fit these latent representations using Gaussian mixture models. A GMM assumes that the data is generated from a mixture of k Gaussian distributions, each with its own mean $\boldsymbol{\mu}_j$ and covariance matrix $\boldsymbol{\Sigma}_j$ for the j -th component. Mathematically, each data point \mathbf{z} has a probability of belonging to the j -th Gaussian component given by the posterior probability:

$$p_j(\mathbf{z}) = \frac{\pi_j \cdot \mathcal{N}(\mathbf{z} | \boldsymbol{\mu}_j, \boldsymbol{\Sigma}_j)}{\sum_{i=1}^k \pi_i \cdot \mathcal{N}(\mathbf{z} | \boldsymbol{\mu}_i, \boldsymbol{\Sigma}_i)},$$

where π_j is the mixing coefficient for the j -th Gaussian component, and $\mathcal{N}(\mathbf{z} | \boldsymbol{\mu}_j, \boldsymbol{\Sigma}_j)$ represents the Gaussian distribution with mean $\boldsymbol{\mu}_j$ and covariance $\boldsymbol{\Sigma}_j$. We denote $\mathbf{p}(\mathbf{z}) = [p_1(\mathbf{z}), p_2(\mathbf{z}), \dots, p_k(\mathbf{z})]$ as the probability vector. To identify data points near the decision boundary, we focus on those points for which the posterior probabilities $\mathbf{p}(\mathbf{z})$ are similar across multiple Gaussian components, indicating that they are near the boundary between different clusters. Specifically, for each data point \mathbf{z} , we calculate the difference between the highest and the second-highest posterior probabilities: $\Delta p = |p_1(\mathbf{z}) - p_2(\mathbf{z})|$, where $p_1(\mathbf{z})$ and $p_2(\mathbf{z})$ are the highest and second-highest posterior probabilities, respectively. Data points with the smallest Δp values are selected, as they are more likely to be near decision boundaries. Finally, the top $\alpha|\mathcal{S}_u|$ unlabeled data with the smallest Δp values are used to form the selected subset. As will be illustrated in Section 5, the robustness performance of SSAT can be largely maintained when using LCS-KM and LCS-GMM to select a small subset of unlabeled data (e.g., $\alpha = 10\%$ or $\alpha = 20\%$). More detailed discussions of the difference between these data selection schemes are provided in Section 6.1, where we visualize the selected unlabeled data in a two-dimensional latent space.

5 Experiments

In this section, we comprehensively evaluate the performance of our proposed data selection schemes, as described in Algorithms 1 and 2, using two widely recognized image benchmarks: SVHN [25] and CIFAR-10 [2] (Section 5.2). Following existing literature, we consider ℓ_∞ -norm bounded perturbations with $\epsilon = 0.015$ on SVHN and $\epsilon = 0.031$ on CIFAR-10. We also highlight the computational advantages of our methods, particularly their ability to reduce the convergence time of SSAT algorithms (Section 5.3). Furthermore, we assess the generalizability of our techniques by applying them to a real-world medical dataset, demonstrating the applicability of our methods beyond standard image benchmarks (Section 5.4).

5.1 Experimental Settings

First, we introduce the necessary details to understand our experimental results. All the remaining details for reproducing our experiments are provided in Appendix B.

Dataset. For the image benchmark experiments, the proposed selection schemes are initially applied to external unlabeled datasets, following the implementation protocols outlined by Carmon et al. [6]. For the SVHN experiments, models are trained on 73K labeled digit images from the original SVHN dataset, supplemented by 531K additional unlabeled SVHN images. Specifically, the CIFAR-10 dataset comprises 50K labeled training images and 10K labeled test images, with models trained using SSAT augmented by an external unlabeled dataset \mathcal{S}_u containing 500K images sampled from the 80M Tiny Images (80M-TI) dataset. To assess the generalizability of our selection schemes, we further evaluate SSAT algorithms using 1M synthetically generated images created by the Denoising Diffusion Probabilistic Model (DDPM) for both CIFAR-10 and SVHN, following the protocols described by Goyal et al. [15].

Configuration. We primarily conduct experiments on SSAT using WideResNet architectures. We train models using TRADES [45] on both labeled and unlabeled data coupled with pseudo labels generated by the intermediate model. In Section 6.3, we evaluate the sensitivity of our methods for varying ℓ_∞ perturbation size, PGD-based adversarial training with varying attack steps, and ℓ_2 perturbations. To standardize training, an epoch is defined as processing 50K data points, regardless of the total dataset size. This is achieved by calculating the required number of batches to cover 50K data points based on the batch size. This approach, adopted in prior works [6, 15], ensures that training time per epoch remains consistent across datasets of varying sizes.

SSAT. For experiments with external unlabeled data, SSAT models are trained for a total of 200 epochs, whereas experiments with generated data extend to 400 epochs. To evaluate the performance of each data selection scheme, models are saved every 25 epoch of SSAT, and the model achieving the highest robust accuracy is selected as the “best” model. This approach aligns with the early stopping practices commonly used in adversarial ML literature [28, 45]. In experiments with external data and selection ratios $\alpha \in \{10\%, 20\%\}$, we consistently observe peak robust accuracy around 100 epochs for CIFAR-10 and 75 epochs for SVHN. Conversely, when no data selection scheme is applied, peak performance is delayed to approximately 200 epochs. Total training time is reported as the duration required to achieve the best model performance.

Intermediate Model. As a foundational step, the proposed selection schemes require training an intermediate model that utilizes the same architecture as the final model. This intermediate model is trained using standard supervised learning for 100 epochs, with training on the WRN-28-10 architecture taking approximately 54 minutes and 43 seconds. Notably, this time is excluded from the reported training durations presented in the results table. The intermediate model fulfills two critical roles: it not only facilitates the pseudo-labeling of unlabeled data but also constitutes a necessary component for the implementation of any data selection strategy. As such, this training step is integral to the overall workflow, irrespective of whether a specific selection method is employed.

Table 1: Comparison results of self-supervised adversarial training performance under different unlabeled data selection schemes and varying ratios on two image benchmarks. For SVHN, we consider ℓ_∞ perturbations with $\epsilon = 0.015$ and train models on Wide ResNet 16-8. For CIFAR-10, we consider ℓ_∞ perturbations with $\epsilon = 0.031$ and train models on Wide ResNet 28-10.

Dataset	Ratio α	Method	External Unlabeled				DDPM-Generated				
			Clean (%)	PGD (%)	AA (%)	Time (h)	Clean (%)	PGD (%)	AA (%)	Time (h)	
SVHN	0%	No Sel.	94.4	75.6	68.3	2.62	94.4	75.6	68.3	2.62	
	100%	No Sel.	97.1	86.0	75.3	8.38	97.4	86.3	75.2	17.41	
	1%	Random	94.2	78.4	70.3	3.28	95.1	80.3	70.5	3.28	
		PCS	95.4	81.8	71.6	3.75	95.4	81.5	71.5	4.08	
		LCS-GMM	95.1	81.8	72.1	3.97	95.6	81.2	71.8	4.27	
		LCS-KM	95.2	82.7	72.9	3.90	96.4	82.4	72.6	4.18	
	10%	Random	95.3	82.0	73.0	3.28	95.6	83.6	72.4	3.28	
		PCS	96.1	82.8	74.2	3.85	95.3	84.0	73.5	4.08	
		LCS-GMM	96.2	83.0	74.3	3.97	95.5	84.1	74.1	4.27	
		LCS-KM	96.1	86.3	75.2	3.90	96.6	86.6	74.8	4.18	
	20%	Random	96.2	82.3	73.2	3.28	96.3	84.6	74.0	3.28	
		PCS	96.3	83.9	74.7	3.75	96.6	85.4	74.5	4.08	
		LCS-GMM	96.4	84.3	75.0	3.97	95.8	85.5	74.7	4.27	
		LCS-KM	96.2	86.6	75.1	3.90	96.7	87.2	75.3	4.18	
	CIFAR-10	0%	No Sel.	84.9	55.4	49.2	10.69	84.9	55.4	49.2	10.69
		100%	No Sel.	89.7	62.5	58.6	28.50	85.7	61.8	58.4	57.13
1%		Random	83.2	54.5	49.8	14.25	83.3	54.3	49.6	14.25	
		PCS	84.9	55.4	51.5	14.73	84.3	55.2	50.7	15.16	
		LCS-GMM	84.2	55.1	52.1	14.89	85.8	54.6	51.8	15.36	
		LCS-KM	85.6	56.4	52.9	14.78	85.9	56.1	52.5	15.27	
10%		Random	85.2	56.0	52.4	14.25	85.0	56.5	52.6	14.25	
		PCS	85.3	56.9	53.7	14.73	85.4	56.9	54.1	15.16	
		LCS-GMM	85.9	57.1	54.2	14.89	85.8	57.1	54.5	15.36	
		LCS-KM	87.2	58.2	55.3	14.78	86.1	58.0	55.8	15.27	
20%		Random	87.1	57.5	54.2	14.25	85.4	57.2	54.2	14.25	
		PCS	87.0	57.9	54.5	14.73	85.6	58.0	55.0	15.16	
		LCS-GMM	87.0	58.2	55.5	14.89	85.9	58.6	55.8	15.36	
		LCS-KM	88.7	60.7	57.8	14.78	85.5	60.2	57.2	15.27	

Evaluation Metric. To evaluate model robustness, we primarily focus on using multi-step PGD attacks (PGD) [22] due to their wide adoption in existing adversarial ML literature. We also report the robust accuracy using AutoAttack (AA) [10] in our main experiments on image benchmarks for more rigorous evaluation and the model’s clean accuracy on normal inputs (Clean) as a reference.

5.2 Main Evaluation on Image Benchmarks

SVHN. Our SVHN evaluation results, summarized in Table 1, demonstrate the efficacy of SSAT algorithms with unlabeled data using various selection schemes and $\alpha \in \{0\%, 1\%, 10\%, 20\%, 100\%\}$ trained on a WRN-16-8 architecture. Specifically, employing the LCS-KM selection strategy with 10% or 20% of the additional data achieves robust accuracies of 86.3% and 86.6%, respectively, which closely approximate the 86.0% robustness achieved using the entire unlabeled dataset. In contrast, random selection with 20% of the data yields a robust accuracy of only 82.3%, underscoring the superior

efficacy of informed selection strategies such as LCS-KM. The robust accuracies evaluated using AutoAttack (i.e., the “AA” column of Table 1) demonstrate similar patterns compared to that using multi-step PGD Attacks (i.e., the “PGD” column of Table 1). Additionally, alternative methods, including PCS and LCS-GMM, consistently outperform random selection, reinforcing the robustness and adaptability of the proposed data selection framework. Notably, the robustness of models trained using SSAT peaks when the boundary ratio parameter β is inversely proportional to the selection ratio α , suggesting that smaller β values are favorable as the data inclusion proportion increases. We provide detailed analyses and discussions of these ratio hyperparameter configurations in Section 6.2.

We also note that the use of ground-truth labels reveals negligible differences compared to pseudo-labeled data, indicating that the primary performance improvements stem from the proposed data selection strategy rather than label accuracy (see Table 4 in Appendix D.2 for details). Additionally, experiments with 1M data

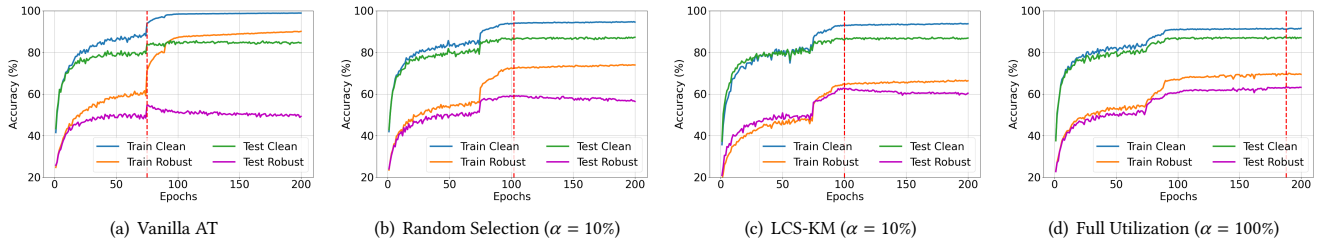


Figure 1: Illustration of standard and robust accuracy curves of SSAT on CIFAR-10 with different settings of selected unlabeled data: (a) No extra data, (b) random selection with $\alpha = 10\%$, (c) LCS-KM with $\alpha = 10\%$, and (d) utilizing all 500K unlabeled images.

points generated using DDPM for SSAT [15] highlight that selecting only 10%–20% of data through LCS-KM achieves comparable performance to utilizing the full unlabeled dataset, with LCS-KM consistently demonstrating superior results. Importantly, training SSAT with selected data requires only 75 epochs to optimize robust accuracy, whereas training with the full dataset demands up to 400 epochs. This significant reduction in computational cost further underscores the practical advantages of the proposed selection methodology, which will be elaborated in Section 5.3.

CIFAR-10. For CIFAR-10 experiments, we adopt the WRN-28-10 architecture to train models using self-supervised adversarial training algorithms. To assess the generalizability of our observations, we also conduct ablation studies on a ResNet-18 architecture, which are detailed in Table 5 in Appendix D.4). The impact of varying proportions, α , of pseudo-labeled unlabeled data was analyzed, revealing that selecting 20% of the external data using LCS-KM achieved a robust accuracy of 60.7%, comparable to the 61.2% obtained with the entire dataset. In contrast, the random selection of the same proportion yielded only 57.8%, underscoring the advantages of strategic data selection techniques such as LCS-KM. Building on the SVHN experiments, we extend our analysis to CIFAR-10 with synthetically generated data. Using 1 million images generated by DDPM [15], we discover that utilizing just 20% of the generated data via LCS-KM resulted in performance metrics nearly identical to those achieved with the full dataset. These trends are consistent across experiments with ℓ_2 perturbations (see Figure 6 for evidence).

Our findings emphasize the robustness and adaptability of the proposed data selection schemes, especially for LCS-KM, even under varying experimental configurations. In terms of computational efficiency, CIFAR-10 experiments highlight the significant advantages of data selection. When leveraging selected external unlabeled data, optimal robust performance was achieved after 100 epochs of training. By contrast, using the full unlabeled or generated datasets without selection required extended training durations of 200 and 400 epochs, respectively, to reach comparable performance. These results validate the efficacy of our latent clustering-based selection approach in enhancing self-supervised adversarial training (SSAT). The proposed method not only maintains the robust accuracy of the final model, θ_{final} , but also substantially reduces computational costs and accelerates the training process, underscoring its practical utility and scalability in adversarial training frameworks. Table 3 in Appendix C summarizes the comparisons, showcasing that

LCS-KM improves model robustness while significantly improving the efficiency of SSAT algorithms with full unlabeled data.

5.3 Computational Benefits

As suggested by the runtime comparisons depicted in Table 1, utilizing smaller, carefully selected unlabeled data can significantly reduce the overall computation costs of SSAT while maintaining competitive, robust accuracy. This section further visualizes the learning curves of SSAT and discusses the computational benefits associated with our proposed methods.

Figure 1 depicts the learning curves of vanilla AT and SSAT algorithms on CIFAR-10 with varying ratios of unlabeled data selected from TinyImages. In our setup, one training epoch corresponds to processing 50K data points, with 10 steps for PGD training and 20 for PGD testing. When no additional data is utilized, as shown in Figure 1(a), the highest robust test accuracy is achieved after approximately 75 epochs. As illustrated in Figures 1(b) and 1(c), incorporating 10% additional data, whether through random selection or curated approaches, extends the optimal convergence point to approximately 100 epochs. In contrast, as depicted in Figure 1(d), leveraging 100% of the unlabeled data delays the achievement of peak accuracy to around 185 epochs. These findings suggest that including extra unlabeled data in SSAT increases computational demands, as evidenced by the longer training convergence time. Strategic selection reduces redundancy in the dataset, allowing the model to achieve optimal performance with fewer training epochs.

Specifically, we observe that the size of the selected unlabeled dataset plays a critical role in determining the time required for the model to achieve peak accuracy. Larger unlabeled datasets usually extend the convergence times of SSAT, whereas smaller datasets facilitate faster convergence, allowing the model to reach optimal accuracy earlier in training. However, continued training beyond this point often leads to robust overfitting. Early stopping offers a computational advantage in scenarios with limited datasets by preventing overfitting with reduced training durations. Nevertheless, early stopping proves less effective in SSAT when working with large-scale unlabeled datasets, as longer training is necessary to achieve peak performance. To mitigate these challenges, selecting a smaller yet strategically curated subset of data significantly reduces the dataset size, enabling faster convergence and minimizing overall training time. These findings underscore the computational benefits of our proposed data selection schemes, providing a practical solution to the challenges of SSAT with extensive datasets.

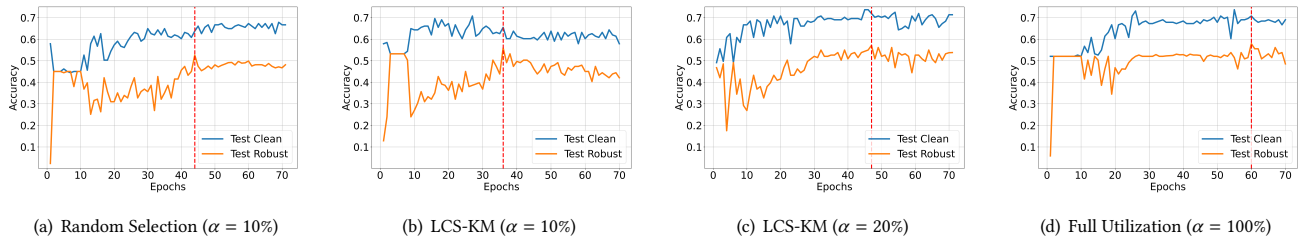


Figure 2: Illustration of testing-time standard and robust accuracy curves of SSAT algorithms with labeled data from the COVIDGR dataset and unlabeled data selected from the CoronaHack dataset. The unlabeled data is incorporated in SSAT with different selection schemes and ratios: (a) random selection with $\alpha = 10\%$, (b) LCS-KM with $\alpha = 10\%$, (c) LCS-KM with $\alpha = 20\%$, and (d) utilizing all unlabeled data corresponding to $\alpha = 100\%$.

5.4 Application to Real-World Medical Data

We extend our study to a real-world healthcare application with COVID-19-related datasets. Specifically, the COVIDGR dataset [36] is utilized as the labeled dataset, and the CoronaHack dataset [14] serves as the source of unlabeled data. This extension allowed us to validate the efficacy of the proposed methods in a domain where data scarcity and model robustness are critical considerations.

Setting. The experimental setup consists of multiple stages, leveraging both datasets in conjunction with ResNet-18 as the base model. The COVIDGR dataset contains 852 chest X-ray images evenly distributed across two classes: 426 COVID-19 positive cases (confirmed via RT-PCR testing) and 426 negative cases. This dataset was split into an 80% training set and a 20% test set for evaluation purposes. The CoronaHack dataset, which comprises 5,910 chest X-ray images, is divided into an 89% training set and an 11% test set. This dataset has an imbalanced class distribution, with 73% of the images classified as COVID-19 positive and 27% as negative (non-COVID). For our experiments, we strategically select a subset of the training data from the CoronaHack dataset as unlabeled data to assess the effectiveness of our adversarial robustness techniques. We applied the LCS-KM selection strategy to identify and incorporate a minimal yet representative subset of unlabeled data from the CoronaHack dataset into the training process. This approach enabled us to maintain robust model performance while significantly reducing the volume of external data required. The models are trained on SSAT with varying unlabeled data selection schemes using a ResNet-18 architecture. We consider ℓ_∞ perturbations with $\epsilon = 0.1$ and vanilla PGD-based adversarial training.

Result Analysis. The results of our experiments confirm the effectiveness of strategic data selection in enhancing robust accuracy and optimizing training efficiency. For instance, using LCS-KM to select 10% of the unlabeled data achieved a robust accuracy of 56%, compared to 53% when the same proportion was selected randomly, as shown in Figures 2(a) and 2(b). Additionally, smaller, strategically selected datasets led to faster convergence, underscoring the benefits of early stopping. Specifically, the best accuracy of 56% was reached at epoch 36 when using 10% of the data selected with LCS-KM in Figure 2(b). Figure 2(c) shows that incorporating 20% of the data with LCS-KM improved the accuracy to 57% at epoch 47. In contrast, training on the entire unlabeled dataset (i.e., $\alpha = 100\%$) required 60 epochs to achieve the highest robust accuracy of 58%

depicted in Figure 2(d). These findings demonstrate that smaller but strategically selected subsets of data can achieve robust accuracy comparable to that of the full dataset while significantly reducing computational time and memory requirements. The success of our approach in this real-world application highlights its practical relevance, particularly in medical diagnostics, where labeled data is limited, yet robust model performance is essential.

6 Additional Analyses

In this section, we conduct additional analyses and experiments to assess the generalizability of our proposed method. We start by visualizing and comparing the latent-space behavior of PCS, LCS-KM, and LCS-GMM to evaluate their effectiveness in selecting critical data points (Section 6.1). Next, we explore the influence of key ratio hyperparameters in our data selection schemes on the robustness performance achieved by SSAT (Section 6.2). Additionally, we evaluate the flexibility of our method across various adversarial training algorithms and perturbation configurations (Section 6.3). Finally, we examine the impact of intermediate model quality, particularly under the regime with insufficient labeled data (Section 6.4). Without explicit mention, we use our LCS-KM method for selecting critical unlabeled data, as it derives the best-performing model when integrated with SSAT as suggested by Table 1.

6.1 Comparative Visualizations

To facilitate a comprehensive understanding of the proposed data selection schemes, we perform a comparative visualization using the TinyImages dataset in the latent space. The latent representations, extracted from the penultimate layer of a pre-trained WRN-28-10 model on CIFAR-10, encode high-dimensional feature embeddings that capture the data’s underlying structure. To render these high-dimensional features interpretable, we employ a two-step dimensionality reduction process that balances the retention of global structure and the visualization of local relationships.

Setting. The first step in this two-step pipeline is *Principal Component Analysis* (PCA). By reducing the dimensionality of the latent features to 50 components, PCA retains the majority of the variance within the data. This step ensures that the global structure of the feature space is preserved, maintaining the relative distances and relationships that reflect the overall organization of the data [12].

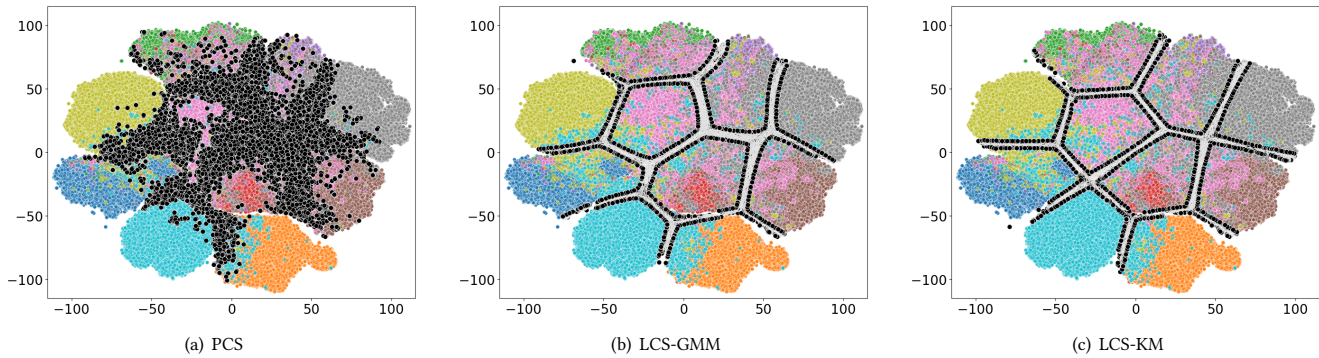


Figure 3: Visual comparison of selection techniques on TinyImages dataset in the latent space. Each subplot represents a different method: (a) PCS identifies points with the lowest classification confidence, highlighting areas where the model is most uncertain within the ten-class latent representation, (b) LCS-GMM illustrates probability contours from Gaussian Mixture Models, with selected points emphasizing regions of overlapping probabilities among the ten class clusters, and (c) LCS-KM highlights points selected near decision boundaries across ten classes based on k-means clustering in the latent space.

PCA also acts as a preprocessing step, making the subsequent visualization process more efficient and effective. In the second step, we apply *t-Distributed Stochastic Neighbor Embedding* (t-SNE) to project the 50-dimensional PCA-reduced features into a two-dimensional space. Unlike PCA, which emphasizes preserving variance, t-SNE is designed to maintain local relationships among data points [41]. This combination of PCA and t-SNE allows us to visualize the latent feature space in a manner that is both interpretable and faithful to the original high-dimensional structure.

After deciding on the two-dimensional latent space, we visualize the selected unlabeled data using our proposed schemes: PCS, LCS-KM, and LCS-GMM. To ensure methodological rigor and consistency, we strictly adhere to the procedures outlined in Algorithms 1 and 2 for implementing the data selection techniques. The ratio hyperparameters α and β are set to 0.1 and 1, respectively. Importantly, these parameters influence the specific distribution of selected points but do not alter the overall interpretability of the visualizations, ensuring that the comparative analysis remains robust by their precise values.

PCS. Figure 3 presents the visualization results, where each color represents the label class predicted by the intermediate model for the corresponding unlabeled point, and the highlighted black dots indicate the data points selected by the respective selection strategy. Our visualization results largely explain why our LCS-KM method consistently achieves the best robustness performance when incorporated in SSAT across various experimental settings. In particular, PCS adopts a purely confidence-based selection strategy, choosing the globally lowest confidence points without considering their distribution within or across classes. Although this direct approach is appealing for its simplicity, it can inadvertently prioritize noisy outliers or ambiguous samples that offer limited benefit for refining the decision boundary. As the number of classes grows and data complexity increases, this scattershot selection tends to yield a more disorganized set of points, as shown in Figure 3(a). This amplifies PCS’s shortcomings compared to the more structured sampling of LCS-KM or the probabilistic clustering offered by LCS-GMM. Thus,

PCS often dedicates training efforts to less informative or highly noisy examples, resulting in weaker robustness improvements.

LCS. LCS-GMM relies on fitting Gaussian distributions to the latent representations. Although this probabilistic approach can effectively capture regions where classes overlap, it inherently presupposes that local data clusters follow (approximately) Gaussian distributions, an assumption that may fail in real-world settings characterized by irregular or noisy data. As a result, LCS-GMM’s contours can become misaligned with the true underlying structure, leading to less accurate localization of essential boundary points [33]. A closer look at the selected boundary samples in Figure 3(b) also reveals that the region these points occupy is broader and less tightly focused on the decision boundary, making it harder to capture truly critical examples for training. Due to the concentration, selected data points overlap with each other in the two-dimensional visualization space. In some instances—such as the cyan region in the figure—LCS-GMM fails to cover as many relevant boundary samples as LCS-KM, further underscoring the latter’s advantage in both coverage and precision.

Finally, our best-performing LCS-KM method emphasizes leveraging the latent-space clustering structure to identify critical decision boundary regions in a more balanced manner. By partitioning the data representations into multiple k-means clusters, LCS-KM systematically locates the points of lowest classification confidence within each cluster, illustrated in Figure 3(c), thereby ensuring that the algorithm focuses on diverse boundary-adjacent regions. This cluster-based approach yields a fine-grained analysis of local uncertainties and avoids the risk of overcommitting to isolated, potentially noisy areas in the latent space.

6.2 Hyperparameter Sensitivity

The efficacy of our selection strategies critically relies on several key hyperparameters, including β that controls the balance between boundary-adjacent unlabeled data and the remaining data points, the proportion of selected unlabeled data α , and the per-batch ratio of extra to original data γ . We record model robust accuracy by

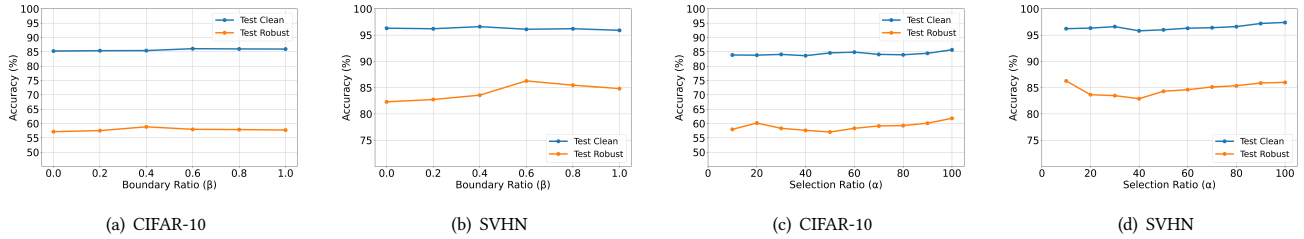


Figure 4: Illustration of SSAT performance using our LCS-KM method with varying boundary and selection ratio parameters with respect to: (a) and (c) DDPM-generated CIFAR-10 data with $\alpha = 20\%$; (b) and (d) 531K extra SVHN data with $\alpha = 10\%$. For each figure, we vary the considered ratio parameter in the x-axis while keeping all the remaining hyperparameters fixed.

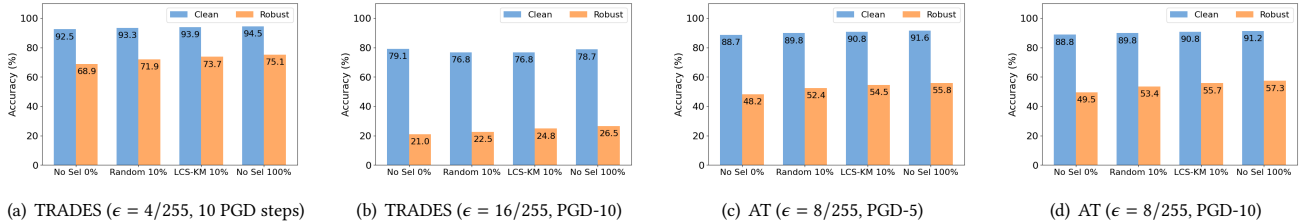


Figure 5: Illustration of SSAT performance on CIFAR-10 using LCS-KM under ℓ_∞ perturbations under various configurations: TRADES using 10 PGD steps with (a) $\epsilon = 4/255$ and (b) $\epsilon = 16/255$; AT with $\epsilon = 8/255$ using (c) 5 PGD steps and (d) 10 PGD steps.

varying each parameter to provide guidelines on how to choose these hyperparameters optimally. Due to page limits, experimental results with varying values of γ are deferred to Appendix D.1.

Ratio of Boundary Points β . Concentrating exclusively on points near the decision boundary can result in an excessive number of points close to the boundary and too few farther away, leading to overfitting. To mitigate this, we choose a combination of points, with some near the boundary and others further away. The proportion of these selections is determined by the value of β . We conduct experiments with different β values to assess their impact on robust accuracy. Figure 4(a) illustrates how robust accuracy varies with β on the CIFAR-10 dataset using 20% generated data from DDPM, which is approximately four times the size of the original dataset. In this scenario, the optimal robust accuracy is achieved when β is 0.4, meaning 40% of the selected points are near the boundary, while 60% are farther away. Figure 4(b) illustrates how robust accuracy varies with β on the SVHN dataset using 10% extra data from the same dataset. Here, due to the smaller amount of external data, selecting points near the boundary results in a lower risk of overfitting. Consequently, the highest robust accuracy is observed when β is 0.6 with 60% of the points near the boundary and 40% farther away. Therefore, the ideal value of β depends on the amount of external data added and the ratio of external to original data. When more external data is added, a smaller β , i.e., fewer points near the boundary, may yield better robust accuracy. Conversely, choosing a larger β is favorable with less extra unlabeled data.

Ratio of Selected Unlabeled Data α . Figures 4(c) and 4(d) illustrate how the performance varies with selection ratio α for CIFAR-10 and SVHN, respectively. We analyze how the quantity of extra data influences the effectiveness of our data-selection method, which is designed to prioritize data points located near decision

boundaries. When the external data supply is limited, our algorithm excels by selecting a higher proportion of boundary-adjacent data, achieving a balanced selection that enhances robust accuracy. However, as the volume of external or generated data increases, the algorithm’s focus on boundary points can inadvertently lead to overfitting, diminishing the improvement gained on the model’s generalization ability. Interestingly, as the data volume continues to grow and more points are added, the performance begins to improve once again, suggesting that the initial overfitting is mitigated by the sheer abundance of data, leading to a recovery in accuracy.

6.3 Further Exploration of Generalizability

All experiments in this section are conducted on CIFAR-10. We compare four different settings: random selection with α ratio of unlabeled data, selecting α ratio using LCS-KM, using only labeled data (i.e., $\alpha = 0\%$), and using the entire dataset (i.e., $\alpha = 100\%$).

Perturbation Size. We consider external data from TinyImages as the unlabeled dataset. We investigate the effect of varying the ℓ_∞ perturbation size ϵ , setting it to $4/255$ and $16/255$ while keeping TRADES as the adversarial training algorithm similar to the experiments in Table 1. The results are depicted in Figures 5(a) and 5(b), suggesting that our LCS-KM method is highly effective compared with random selection and no selection, almost approaching the robust accuracies achieved by full utilization of unlabeled data. The trends are shown to be consistent across varying perturbation sizes.

Adversarial Training. We explore the impact of replacing TRADES with vanilla AT as the training algorithm. Similarly, we use external data from TinyImages as the unlabeled dataset. The results for PGD-based AT are shown in Figure 5(d). Additionally, we reduce the number of PGD steps from 10 to 5, and the outcomes are summarized in Figure 5(c). Across all configurations, our LCS-KM

Table 2: Performance of intermediate models trained using different schemes, including self-supervised learning (SSL), pre-trained CLIP, and fully-supervised methods, on CIFAR-10 under varying ratios of labeled data. We also present the corresponding performance of the final model produced by SSAT with LCS-KM, where the ratio of selected unlabeled data α is set at 10%.

Labeled Ratio	Intermediate Model		Final Model (LCS-KM, $\alpha = 10\%$)	
	Training Method	Clean Acc (%)	Clean Acc (%)	Robust Acc (%)
1%	SSL (5% unlabeled)	78.8	82.9	39.8
	pre-trained CLIP	86.8	83.9	40.5
10%	SSL (5% unlabeled)	82.9	85.0	42.4
	pre-trained CLIP	86.8	85.3	43.2
20%	SSL (5% unlabeled)	87.0	87.2	48.3
	pre-trained CLIP	86.8	85.6	47.7
100%	fully-supervised	90.5	86.2	58.2
	pre-trained CLIP	86.8	86.5	57.4

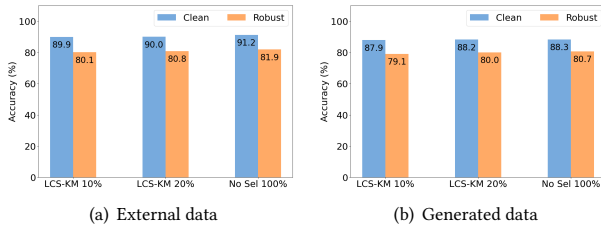


Figure 6: Illustration of SSAT performance on CIFAR-10 under ℓ_2 perturbations with $\epsilon = 128/255$ using LCS-KM by varying α : (a) external TinyImages and (b) DDPM-generated data.

selection consistently outperforms random selection and achieves accuracy comparable to using the entire labeled dataset, suggesting the generalizability and robustness of our methods.

ℓ_2 Perturbations. We further evaluate the performance of LCS-KM under ℓ_2 perturbations with size $\epsilon = 128/255$. In this experiment, we augment CIFAR-10 with either external unlabeled data sourced from Tiny-ImageNet or synthetic data generated via DDPM. We consider three configurations of selecting 10%, 20%, and 100% extra unlabeled data. Our findings are shown in 6(a) and 6(b), revealing that selecting 20% unlabeled data achieves nearly equivalent robust accuracy compared to using the full dataset with $\alpha = 100\%$. These results again confirm the efficiency and effectiveness of LCS-KM when adopted in self-supervised adversarial training algorithms.

6.4 Low Labeled Data Regime

We further study how the choice of the intermediate model and the amount of labeled data impact the final performance. For all experiments, we use a subset of the CIFAR-10 dataset as labeled data, supplemented with 10% of data selected from a pool of 500K unlabeled images sourced from Tiny-ImageNet. This additional data is selected using the intermediate model. The amount of unlabeled data remains constant across experiments, while the quantity of labeled data is varied. The intermediate model is trained using self-supervised learning (SSL) with a 5% randomly selected subset of

the unlabeled dataset, as long as the labeled data ratio is low. Additionally, we include a pre-trained CLIP model [27] as an alternative intermediate model for comparison. The results of these experiments are presented in Table 2. The intermediate model’s quality significantly impacts the final model’s robust accuracy. In low-label regimes (e.g., 1% or 10%), models trained using our intermediate model yield comparatively lower robust accuracy than those leveraging the pre-trained CLIP model. However, as the amount of labeled data for the intermediate model increases (e.g., 20% or 100%), the final model results are similar to or better than those of its counterparts based on the CLIP intermediate model. This trend demonstrates the effect of the intermediate model on the final robust accuracy. These observations underscore the importance of having a strong intermediate model for robust performance. Additionally, we find that pre-trained models like CLIP can be a good alternative to training an intermediate model, especially in low-label regimes. Detailed experiment results and discussions on the pre-trained CLIP intermediate model are provided in Appendix D.3.

6.5 Further Discussion

Our study introduces strategic data selection methods, including Latent Clustering-Based Selection with k-means (LCS-KM), Latent Clustering-Based Selection with Gaussian Mixture Models (LCS-GMM), and prediction confidence-based selection, to improve the efficiency of self-supervised adversarial training. These approaches tackle key challenges in adversarially robust learning, particularly the significant memory and computational overhead of existing methods. By prioritizing boundary-adjacent data, these processes aim to enhance model robustness. However, these methods assume that the model’s latent representations are reliable for clustering and confidence evaluation, an assumption that may falter in the case of undertrained or poorly calibrated models. While these approaches effectively reduce the volume of unlabeled data required for training, their performance can be sensitive to hyperparameter configurations, such as the balance between boundary and non-boundary points and the size of the unlabeled dataset. By focusing on challenging examples near the decision boundary, these selection methods naturally address some aspects of robust overfitting

and support robust generalization. Nevertheless, deeper investigation is required to fully comprehend how these strategies influence decision boundary geometry and the model’s capacity for robust generalization. Combining these selection techniques with fast and efficient adversarial example generation methods, such as fast and free adversarial training, holds promise for further accelerating the training process while preserving robust performance.

7 Conclusion

In this work, we illustrated the importance of latent clustering-based data selection in improving the efficiency of SSAT while maintaining robust accuracy. Emphasizing boundary data points during selection significantly enhances the model’s overall robustness. For SVHN, we also showed improvement in robust accuracy by adding ground-truth labels to a small set of data. This suggests manually annotating a few unlabeled data points close to the boundary could be a potential future direction to further enhance model robustness with considerations of memory and computational efficiency. Our work opens new avenues for further research, including exploring advanced data selection schemes, making the selection process more interpretable, and investigating the trade-offs between model performance, data selection, and computational costs.

References

- [1] Jean-Baptiste Alayrac, Jonathan Uesato, Po-Sen Huang, Alhussein Fawzi, Robert Stanforth, and Pushmeet Kohli. 2019. Are labels required for improving adversarial robustness? *Advances in Neural Information Processing Systems* 32 (2019).
- [2] Krizhevsky Alex. 2009. Learning multiple layers of features from tiny images. <https://www.cs.toronto.edu/kriz/learning-features-2009-TR.pdf> (2009).
- [3] Battista Biggio and Fabio Roli. 2018. Wild patterns: Ten years after the rise of adversarial machine learning. In *Proceedings of the 2018 ACM SIGSAC Conference on Computer and Communications Security*. 2154–2156.
- [4] Jacob Buckman, Aurko Roy, Colin Raffel, and Ian Goodfellow. 2018. Thermometer encoding: One hot way to resist adversarial examples. In *International conference on learning representations*.
- [5] Nicholas Carlini and David Wagner. 2017. Towards evaluating the robustness of neural networks. In *2017 IEEE Symposium on Security and Privacy (SP)*. Ieee, 39–57.
- [6] Yair Carmon, Aditi Raghunathan, Ludwig Schmidt, John C Duchi, and Percy S Liang. 2019. Unlabeled data improves adversarial robustness. *Advances in neural information processing systems* 32 (2019).
- [7] O. Chapelle, B. Scholkopf, and A. Zien, Eds. 2009. Semi-Supervised Learning (Chapelle, O. et al., Eds.; 2006) [Book reviews]. *IEEE Transactions on Neural Networks* 20, 3 (2009), 542–542. <https://doi.org/10.1109/TNN.2009.2015974>
- [8] Francesco Croce, Maksym Andriushchenko, Vikash Sehraw, Edoardo DeBenedetti, Nicolas Flammarion, Mung Chiang, Prateek Mittal, and Matthias Hein. 2020. Robustbench: a standardized adversarial robustness benchmark. *arXiv preprint arXiv:2010.09670* (2020).
- [9] Francesco Croce and Matthias Hein. 2020. Reliable evaluation of adversarial robustness with an ensemble of diverse parameter-free attacks. In *Proceedings of the 37th International Conference on Machine Learning (Proceedings of Machine Learning Research, Vol. 119)*, Hal Daumé III and Aarti Singh (Eds.). PMLR, 2206–2216. <https://proceedings.mlr.press/v119/croce20b.html>
- [10] Francesco Croce and Matthias Hein. 2020. Reliable evaluation of adversarial robustness with an ensemble of diverse parameter-free attacks. In *ICML*.
- [11] Hadi M Dolatabadi, Sarah M Erfani, and Christopher Leckie. 2023. Adversarial coresets selection for efficient robust training. *International Journal of Computer Vision* 131, 12 (2023), 3307–3331.
- [12] Felipe L Gewers, Gustavo R Ferreira, Henrique F De Arruda, Filipi N Silva, Cesar H Comin, Diego R Amancio, and Luciano da F Costa. 2021. Principal component analysis: A natural approach to data exploration. *ACM Computing Surveys (CSUR)* 54, 4 (2021), 1–34.
- [13] Ian J Goodfellow, Jonathon Shlens, and Christian Szegedy. 2014. Explaining and harnessing adversarial examples. *arXiv preprint arXiv:1412.6572* (2014).
- [14] Praveen Govi. 2020. Coronahack Chest X-Ray Dataset. <https://www.kaggle.com/datasets/praveengovi/coronahack-chest-xraydataset/data>. Accessed: 2025-01-07.
- [15] Sven Gowal, Sylvestre-Alvise Rebuffi, Olivia Wiles, Florian Stimberg, Dan Andrei Calian, and Timothy A Mann. 2021. Improving robustness using generated data. *Advances in Neural Information Processing Systems* 34 (2021), 4218–4233.
- [16] Chuan Guo, Geoff Pleiss, Yu Sun, and Kilian Q Weinberger. 2017. On calibration of modern neural networks. In *International conference on machine learning*. PMLR, 1321–1330.
- [17] Kaiming He, Xiangyu Zhang, Shaoqing Ren, and Jian Sun. 2016. Deep residual learning for image recognition. In *Proceedings of the IEEE conference on computer vision and pattern recognition*. 770–778.
- [18] Weizhe Hua, Yichi Zhang, Chuan Guo, Zhiru Zhang, and G Edward Suh. 2021. Bullettrain: Accelerating robust neural network training via boundary example mining. *Advances in Neural Information Processing Systems* 34 (2021), 18527–18538.
- [19] Vishal Kaushal, Rishabh Iyer, Suraj Kothawade, Rohan Mahadev, Khoshnav Doctor, and Ganesh Ramakrishnan. 2019. Learning from less data: A unified data subset selection and active learning framework for computer vision. In *2019 IEEE Winter Conference on Applications of Computer Vision (WACV)*. IEEE, 1289–1299.
- [20] Yeachan Kim and Bonggun Shin. 2022. In defense of core-set: A density-aware core-set selection for active learning. In *Proceedings of the 28th ACM SIGKDD Conference on Knowledge Discovery and Data Mining*. 804–812.
- [21] Diederik P Kingma. 2014. Adam: A method for stochastic optimization. *arXiv preprint arXiv:1412.6980* (2014).
- [22] Aleksander Madry, Aleksandar Makelov, Ludwig Schmidt, Dimitris Tsipras, and Adrian Vladu. 2017. Towards deep learning models resistant to adversarial attacks. *arXiv preprint arXiv:1706.06083* (2017).
- [23] Baharan Mirzasoleiman, Jeff Bilmes, and Jure Leskovec. 2020. Coresets for Data-efficient Training of Machine Learning Models. In *Proceedings of the 37th International Conference on Machine Learning (Proceedings of Machine Learning Research, Vol. 119)*, Hal Daumé III and Aarti Singh (Eds.). PMLR, 6950–6960. <https://proceedings.mlr.press/v119/mirzasoleiman20a.html>
- [24] Amir Najafi, Shin-ichi Maeda, Masanori Koyama, and Takeru Miyato. 2019. Robustness to adversarial perturbations in learning from incomplete data. *Advances in Neural Information Processing Systems* 32 (2019).
- [25] Yuval Netzer, Tao Wang, Adam Coates, Alessandro Bissacco, Baolin Wu, Andrew Y Ng, et al. 2011. Reading digits in natural images with unsupervised feature learning. In *NIPS workshop on deep learning and unsupervised feature learning*, Vol. 2011. Granada, Spain, 7.
- [26] Nicolas Papernot, Patrick McDaniel, Xi Wu, Somesh Jha, and Ananthram Swami. 2016. Distillation as a defense to adversarial perturbations against deep neural networks. In *2016 IEEE Symposium on Security and Privacy (SP)*. IEEE, 582–597.
- [27] Alec Radford, Jong Wook Kim, Chris Hallacy, Aditya Ramesh, Gabriel Goh, Sandhini Agarwal, Girish Sastry, Amanda Askell, Pamela Mishkin, Jack Clark, et al. 2021. Learning transferable visual models from natural language supervision. In *International conference on machine learning*. PMLR, 8748–8763.
- [28] Leslie Rice, Eric Wong, and Zico Kolter. 2020. Overfitting in adversarially robust deep learning. In *International Conference on Machine Learning*. PMLR, 8093–8104.
- [29] Ludwig Schmidt, Shibani Santurkar, Dimitris Tsipras, Kunal Talwar, and Aleksander Madry. 2018. Adversarially robust generalization requires more data. *Advances in neural information processing systems* 31 (2018).
- [30] Vikash Sehraw, Saeed Mahloujifar, Tinashe Handina, Sihui Dai, Chong Xiang, Mung Chiang, and Prateek Mittal. 2021. Robust learning meets generative models: Can proxy distributions improve adversarial robustness? *arXiv preprint arXiv:2104.09425* (2021).
- [31] Ozan Sener and Silvio Savarese. 2017. Active learning for convolutional neural networks: A core-set approach. *arXiv preprint arXiv:1708.00489* (2017).
- [32] Ali Shafahi, Mahyar Najibi, Mohammad Amin Ghiasi, Zheng Xu, John Dickerson, Christoph Studer, Larry S Davis, Gavin Taylor, and Tom Goldstein. 2019. Adversarial training for free! *Advances in neural information processing systems* 32 (2019).
- [33] Douglas Steinley and Michael J Brusco. 2011. Evaluating mixture modeling for clustering: recommendations and cautions. *Psychological methods* 16, 1 (2011), 63.
- [34] Ilya Sucholutsky and Matthias Schonlau. 2021. Soft-label dataset distillation and text dataset distillation. In *2021 International Joint Conference on Neural Networks (IJCNN)*. IEEE, 1–8.
- [35] Christian Szegedy, Wojciech Zaremba, Ilya Sutskever, Joan Bruna, Dumitru Erhan, Ian Goodfellow, and Rob Fergus. 2013. Intriguing properties of neural networks. *arXiv preprint arXiv:1312.6199* (2013).
- [36] Siham Tabik, Anabel Gómez-Ríos, José Luis Martín-Rodríguez, Iván Sevillano-García, Manuel Rey-Area, David Chartre, Emilio Guirado, Juan-Luis Suárez, Julián Luengo, MA Valero-González, et al. 2020. COVIDGR dataset and COVID-SDNet methodology for predicting COVID-19 based on chest X-ray images. *IEEE journal of biomedical and health informatics* 24, 12 (2020), 3595–3605.
- [37] Tongzhou Wang, Jun-Yan Zhu, Antonio Torralba, and Alexei A Efros. 2018. Dataset distillation. *arXiv preprint arXiv:1811.10959* (2018).
- [38] Yisen Wang, Difan Zou, Jinfeng Yi, James Bailey, Xingjun Ma, and Quanquan Gu. 2019. Improving adversarial robustness requires revisiting misclassified

- examples. In *International conference on learning representations*.
- [39] Zekai Wang, Tianyu Pang, Chao Du, Min Lin, Weiwei Liu, and Shuicheng Yan. 2023. Better diffusion models further improve adversarial training. In *International Conference on Machine Learning*. PMLR, 36246–36263.
 - [40] Eric Wong, Leslie Rice, and J Zico Kolter. 2020. Fast is better than free: Revisiting adversarial training. *arXiv preprint arXiv:2001.03994* (2020).
 - [41] Jiazhi Xia, Yuchen Zhang, Jie Song, Yang Chen, Yunhai Wang, and Shixia Liu. 2021. Revisiting dimensionality reduction techniques for visual cluster analysis: An empirical study. *IEEE Transactions on Visualization and Computer Graphics* 28, 1 (2021), 529–539.
 - [42] Xiaobo Xia, Jiale Liu, Jun Yu, Xu Shen, Bo Han, and Tongliang Liu. 2022. Moderate coresets: A universal method of data selection for real-world data-efficient deep learning. In *The Eleventh International Conference on Learning Representations*.
 - [43] Sergey Zagoruyko and Nikos Komodakis. 2016. Wide residual networks. *arXiv preprint arXiv:1605.07146* (2016).
 - [44] Runtian Zhai, Tianle Cai, Di He, Chen Dan, Kun He, John Hopcroft, and Liwei Wang. 2019. Adversarially robust generalization just requires more unlabeled data. *arXiv preprint arXiv:1906.00555* (2019).
 - [45] Hongyang Zhang, Yaodong Yu, Jiantao Jiao, Eric Xing, Laurent El Ghaoui, and Michael Jordan. 2019. Theoretically principled trade-off between robustness and accuracy. In *International conference on machine learning*. PMLR, 7472–7482.
 - [46] Jingfeng Zhang, Jianing Zhu, Gang Niu, Bo Han, Masashi Sugiyama, and Mohan Kankanhalli. 2020. Geometry-aware instance-reweighted adversarial training. *arXiv preprint arXiv:2010.01736* (2020).
 - [47] Bo Zhao, Konda Reddy Mopuri, and Hakan Bilen. 2020. Dataset condensation with gradient matching. *arXiv preprint arXiv:2006.05929* (2020).

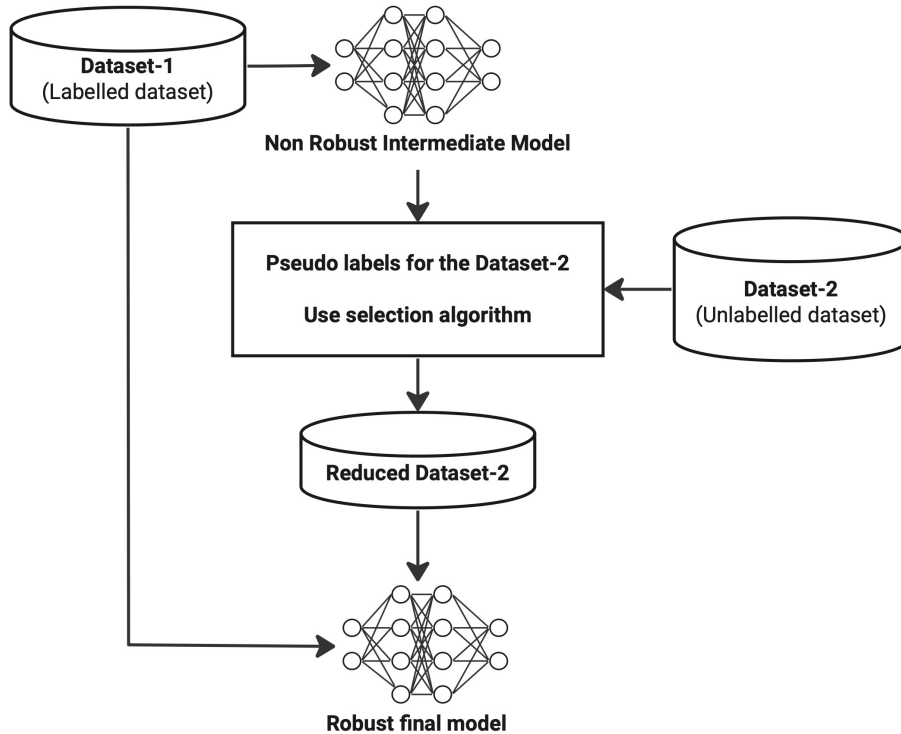


Figure 7: Overview of the training pipeline. An intermediate model is first trained with labeled data and then used to select data from the unlabeled set. Finally, we adopt SSAT to learn a robust model on both the labeled and the reduced unlabeled datasets.

A Overall Training Pipeline

Figure 7 illustrates the overall pipeline, based on the robust self-training framework proposed by Carmon et al. [6]. We first train our intermediate model using the available labeled data and use this intermediate model to select a subsection of our unlabeled or generated data. The final robust training is performed on all the labeled data and a strategically selected subset of the unlabeled or generated data.

B Detailed Experimental Setup

SVHN. SVHN is naturally divided into a core training set comprising approximately 73K images and an extra training set of around 531K images. Initially, the model is trained on the 73K labeled images. To evaluate the generalizability of our selection schemes, we apply it to a synthetic dataset generated using a DDPM model [15].

Configuration. For model training, we adopt a WideResNet 16-8 (WRN-16-8) architecture [43] in all our SVHN experiments. We generate adversarial examples using PGD attacks exactly as implemented by Zhang et al. [45], with step size 0.007, 10-step PGD attack iterations, and ℓ_∞ perturbation magnitude $\epsilon = 0.015$. Hyperparameters are set the same as in Carmon et al. [6] except for the number of epochs. For SVHN, we use a training batch size of 128. All of our experiments that utilize all of the extra 531K data are run for 200 epochs and the experiments with 1M generated data are run for 400 epochs. To prevent overfitting and reduce computational complexity, we run our experiments with selected data for 75 epochs with early stopping. Following prior literature [6], we adopt an SGD optimizer with a weight decay factor of $5 \cdot 10^{-4}$ and an initial learning rate of 0.1 with a cosine learning rate annealing to train the model.

Evaluation. For the attack evaluation to calculate the robust accuracy using PGD attack, we keep the parameters similar to that of Carmon et al. [6] for better comparison. We use step size 0.005, number of attack steps $K = 100$. We evaluate models at $\epsilon = 0.015$, which is the same as the value we used during training. We also use Auto Attack with the same ϵ value as in PGD attack.

CIFAR-10. The CIFAR-10 dataset has 50K labeled images. We use the 80 Million Tiny Images (80M-TI) dataset, of which CIFAR-10 is a manually labeled subset, to obtain extra data. However, most images in 80M-TI do not correspond to CIFAR-10 image categories. Carmon et al. [6] used an 11-way classifier to distinguish CIFAR-10 classes and an 11th “non-CIFAR-10” class using a WideResNet 28-10 model. Each class selected an additional 50K images from 80M-TI using the model’s predicted scores to create a 500K pseudo-labeled dataset, which we used in our experiments. We train the intermediate model with 50K labeled data and use this model to select data from the 500K pseudo-labeled data

Table 3: Comparisons of SSAT methods with different selection schemes based on average efficiency score and robust accuracy. Here, we compute the average of the results for $\alpha = 10\%$ and $\alpha = 20\%$ for our selection methods, and for the “No Selection” method, we use $\alpha = 100\%$, taking the average of the external and generated data results for each setting.

Method	Efficiency Score	Robust Accuracy (%)	
		SVHN	CIFAR-10
Random	1.00	83.1 ± 1.04	56.8 ± 0.59
PCS	0.89	84.0 ± 0.92	57.4 ± 0.53
LCS-GMM	0.87	84.2 ± 0.89	57.8 ± 0.67
LCS-KM	0.88	86.6 ± 0.33	59.3 ± 1.15
No Selection	0.33	86.2 ± 0.15	62.2 ± 0.35

or a synthetic dataset. We perform the same experiments as in SVHN, except that we do not have the ground-truth labels of the additional unlabeled dataset. We also conducted further experiments utilizing 1M synthetical data generated by the DDPM model [15].

Configuration. For our main CIFAR-10 experiments, we use a WideResNet 28-10 (WRN-28-10) [43] architecture to train models. Similar to SVHN experiments, we set step size 0.007, PGD attack iterations as 10 and ℓ_∞ perturbation magnitude $\epsilon = 0.031$. For our adversarial training with ℓ_2 perturbation, we use $\epsilon = 128/255$. In section 6.3 when $\epsilon = 4/255$, we use 0.0035 as the PGD step size. For $\epsilon = 16/255$, we use 0.015 as the PGD step size. Hyperparameters used are the same as in Carmon et al. [6] except for the number of epochs. Here, we use a training batch size of 256. The experiments using all the 500K pseudo-labeled data are run for 200 epochs, and using 1M generated data are run for 400 epochs. For our experiments with limited data, we get the best results at 100 epochs where we early stop the training process. Following prior literature [6], we adopt an SGD optimizer with a weight decay factor of $5 \cdot 10^4$ and an initial learning rate of 0.1 with a cosine learning rate annealing to train the model.

Evaluation. The PGD attack evaluation is conducted similarly to that of Carmon et al. [6] for fair comparisons. We use step size $\alpha = 0.01$, number of attack steps $K = 40$. We consider ℓ_∞ perturbations with $\epsilon = 0.031$, the same as the perturbation magnitude we used during training. For the models trained with ℓ_2 perturbation, we evaluate with ℓ_2 perturbation magnitude $\epsilon = 128/255$. We also use Auto Attack with the same ϵ value as in PGD attack.

Medical Application. Below, we detail the setup employed for our experiments on the medical datasets outlined in Section 5.4. For this experiment, we trained models using a ResNet-18 [17] architecture. We consider ℓ_∞ perturbations with $\epsilon = 0.1$. We set the attack step size to 0.02, and the number of PGD steps to 10. The final model is trained with SSAT using the Adam optimizer [21] with a learning rate of 0.001. We evaluate model robustness with PGD attacks with a step size of 0.02 and 20 attack steps.

C Detailed Comparisons of Different Data Selection Schemes

This section presents a comprehensive comparison of all the selection methods, including the case where no selection is applied. It highlights the tradeoff between performance and efficiency, offering a detailed analysis of the conditions under which each method is most suitable. Table 3 summarizes the performance of SSAT with different data selection strategies in terms of efficiency and robust accuracy. Each method strikes a balance between computational cost and accuracy improvements. Random selection serves as a baseline with minimal computation but lacks precision, while our strategic selection methods prioritize boundary points, which achieve progressively improved performance but with moderate increases in computational demands. Using 100% of the data without selection yields the highest robust accuracy but at a significant computational cost. More specifically, we calculate a normalized efficiency score for each method defined as $\text{Eff Score}_{ij} = \frac{T_{\min,j}}{T_{ij}}$, where $T_{\min,j}$ is the minimum training time for dataset j , and T_{ij} is the actual training time for method i . The overall efficiency score for method i is the average across all datasets computed as $\frac{1}{n} \sum_j \text{Eff Score}_{ij}$, where n denotes the number of datasets and sources considered. Effectiveness is measured by the average robust accuracy across CIFAR-10 and SVHN. In particular, we compute the average of the results for $\alpha = 10\%$ and $\alpha = 20\%$ for our selection methods, and for the no-selection method, we use $\alpha = 100\%$. In all cases, we take the average of the results from both the external and generated data. These metrics are introduced to provide a fair comparison between methods.

D Additional Experiments

D.1 Other Hyperparameter Analysis Details and Results

In Section 6.2, we present a detailed analysis of how accuracies are influenced by different hyperparameter values. In these experiments, we varied one hyperparameter at a time while keeping the others constant. Figure 4(a) illustrates how robust accuracy on the CIFAR-10 dataset changes with β values when 20% additional data is incorporated from the 1M data samples generated by the DDPM model, using a per-batch ratio of 0.3. Figure 4(b) shows the variation in robust accuracy for the SVHN dataset as β changes, with 10% drawn from the SVHN extra dataset and a per-batch ratio of 0.5. In Figure 8(a), we present how robust accuracy for the CIFAR-10 dataset is affected by varying the ratio

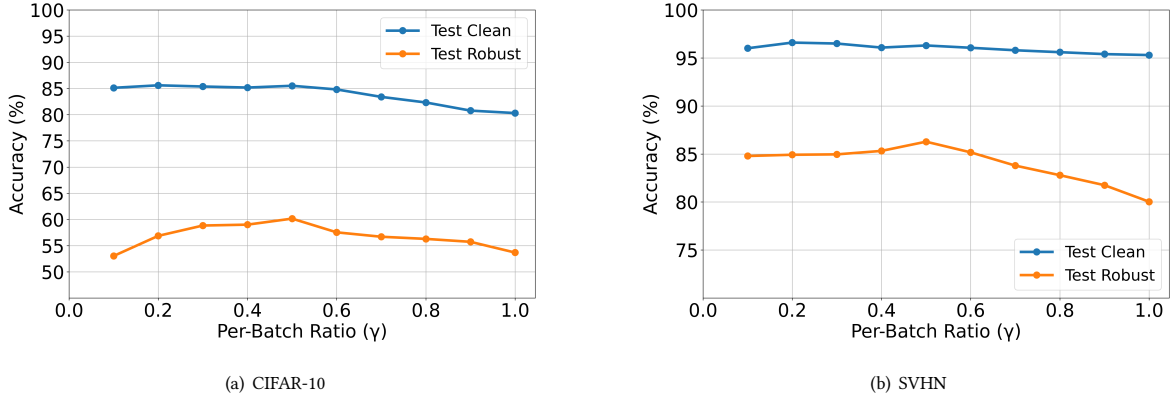


Figure 8: Illustration of clean and robust accuracy curves of SSAT algorithms with LCS-KM by varying per-batch ratio γ , which defines how much labeled and unlabeled data are included in each mini-batch, on: (a) CIFAR-10 with 20% extra unlabeled data selected from 1M generated images using DDPM, and (b) SVHN with 10% selected from the external 531K SVHN images.

Table 4: Comparison results of self-supervised adversarial training algorithms with varying data selection schemes on SVHN. Instead of pseudo labels, the selected unlabeled data are assigned with the ground-truth SVHN labels provided in the dataset.

Ratio α	Method	Clean Accuracy (%)	Robust Accuracy (%)	Number of Epochs
1%	LCS-KM	95.6	82.9	75
10%	Random	96.3	82.7	75
10%	LCS-KM	96.7	86.3	75
20%	LCS-KM	96.4	86.5	75
100%	No Selection	97.5	86.4	200

of per-batch ratio γ when 20% extra data from the 1M generated DDPM samples is used, with β fixed at 0.4. Similarly, Figure 8(b) displays the effect of varying the per-batch ratio on robust accuracy for the SVHN dataset, using 10% data from the SVHN extra dataset and fixing β at 0.6. In addition, Figures 4(c) and 4(d) explore how robust accuracy varies with the amount of data used. For CIFAR-10 in Figure 4(c), the per-batch ratio is set to 0.5, and β is fixed at 0.4. For the SVHN dataset in Figure 4(d), the per-batch ratio is set to 0.5, and β is set to 0.6. We aim to capture the robust accuracy at the optimal epoch in each case, and we observe that for Figures 4(c) and 4(d), as the amount of data increases, the optimal accuracy is reached at a considerably later epoch.

D.2 SVHN with Ground-Truth Labels

We conduct additional experiments to test the performance of our data selection scheme on SVHN with pseudo labels replaced by ground-truth labels for the extra data. Table 4 shows the comparison results. With ground-truth labels, our LCS schemes can achieve similar robust accuracy by selecting just 10% extra data compared with no selection result.

D.3 Pre-Trained CLIP as Intermediate Model

In all our previous experiments, we began by training an intermediate model $f_{\hat{\theta}}$ using the same architecture as the final model θ_{final} . This intermediate model was trained exclusively on the labeled dataset and then used to generate pseudo labels and select a subset from the extra dataset. However, when dealing with generated or external data that already comes with labels, training an intermediate model specifically for selection undermines the selection process’s intended benefits, primarily to reduce computational and time complexity. In addition, in application scenarios where the size of the labeled dataset \mathcal{S}_l is also limited, likely, the intermediate model can not be trained with high accuracy, leading to large amounts of inaccurate pseudo labels.

To address these issues, we study the feasibility of using an alternative pre-trained model in LCS to perform data selection, specifically leveraging the CLIP model for extracting image embeddings [27]. CLIP, trained on a vast array of internet images and text, offers a rich and versatile feature space that can be utilized without additional training. By using the capabilities of pre-trained CLIP, we can bypass the intermediate step of training a model from scratch, thereby streamlining the selection process and further enhancing overall efficiency. This substitution allows us to select a relevant subset without having to train an intermediate model from scratch. Our experiments indicate that

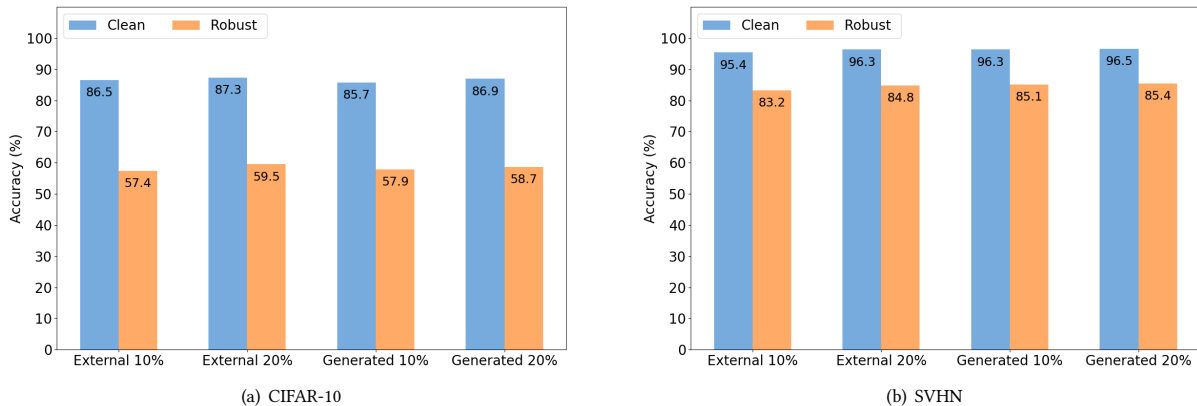


Figure 9: Comparisons of SSAT methods with varying amounts of unlabeled data selected using LCS-KM with the CLIP model on (a) CIFAR-10 and (b) SVHN. We measure both standard and robust accuracies on the corresponding testing labeled dataset.

using CLIP for data selection yields results that are comparable to those obtained using the trained intermediate model, both in terms of standard and robust accuracies. Figure 9 shows our result when using CLIP instead of the previous intermediate model for data selection.

D.4 Resnet-18 Model Architecture

Our main experiments focus on the WidResNet architecture. We further evaluate the performance of SSAT under ℓ_∞ perturbations with $\epsilon = 0.031$ using different data selection schemes and varying selection ratios with external unlabeled data on CIFAR-10 using a ResNet-18 model. Similar to our previous experiments, we train the ResNet-18 model on 50K labeled samples from CIFAR-10 and a chosen subset of data from 500K unlabeled images of Tiny-ImageNet. Our evaluation results are shown in Table 5, which suggests that our proposed LCS methods can greatly improve the efficacy of SSAT on ResNet-18 while achieving comparable robustness performance of “No Selection” with $\alpha = 100\%$.

Table 5: Comparisons of SSAT performance on CIFAR-10 using the ResNet-18 architecture under various configurations. The model training dataset consists of 50K labeled CIFAR-10 images and 500K unlabeled images drawn from Tiny-ImageNet.

Ratio α	Method	Clean Accuracy (%)	Robust Accuracy (%)
1%	Random	79.8	50.6
	PCS	79.4	51.1
	LCS-GMM	78.7	51.6
	LCS-KM	78.1	51.8
10%	Random	82.3	52.0
	PCS	82.1	52.6
	LCS-GMM	82.0	53.2
	LCS-KM	83.3	53.6
20%	Random	82.4	53.1
	PCS	82.1	53.3
	LCS-GMM	82.1	53.7
	LCS-KM	83.1	54.0
100%	No Selection	83.2	54.7